Thrombosis Research 189 (2020) 119–127

Contents lists available at ScienceDirect

Thrombosis Research

journal homepage: www.elsevier.com/locate/thromres

Full Length Article

Targeting of externalized αB-crystallin on irradiated endothelial cells with pro-thrombotic vascular targeting agents: Potential applications for brain arteriovenous malformations

Sinduja Subramanian[a], Zhenjun Zhao[a], Fahimeh Faqihi[a], Georges E. Grau[b], Valery Combes[c], David W. Inglis[d], Vaughan Moutrie[e], Marcus A. Stoodley[a], Lucinda S. McRobb[a,*]

[a] Department of Clinical Medicine, Macquarie University, Sydney 2109, Australia
[b] Department of Pathology, University of Sydney, Sydney 2050, Australia
[c] School of Life Sciences, Faculty of Science, University of Technology, Sydney 2006, Australia
[d] School of Engineering, Macquarie University, Sydney 2109, Australia
[e] Genesis Cancer Care, Macquarie University Hospital, Sydney 2109, Australia

ARTICLE INFO

Keywords:
αB-crystallin
Arteriovenous malformation
Endothelial cells
Ionizing radiation
Thrombosis
Vascular targeting

ABSTRACT

Background: Vascular targeting uses molecular markers on the surface of diseased vasculature for ligand-directed drug delivery to induce vessel occlusion or destruction. In the absence of discriminatory markers, such as in brain arteriovenous malformations (AVMs), stereotactic radiosurgery may be used to prime molecular changes on the endothelial surface. This study explored αB-crystallin (CRYAB) as a radiation induced target and pre-tested the specificity and efficacy of a CRYAB-targeting coaguligand for *in vitro* thrombus induction.

Methods: A parallel-plate flow system was established to circulate human whole blood over a layer of human brain endothelial cells. A conjugate of anti-CRYAB antibody and thrombin was injected into the circuit to compare binding and thrombus formation on cells with or without prior radiation treatment (0–25 Gy).

Results: Radiation increased CRYAB expression and surface exposure in human brain endothelial cells. In the parallel-plate flow system, the targeted anti-CRYAB–thrombin conjugate increased thrombus formation on the surface of irradiated cells relative to non-irradiated cells and to a non-targeting IgG-thrombin conjugate. Fibrin deposition and accumulation of fibrinogen degradation products increased significantly at radiation doses at or above 15 Gy with conjugate concentrations of 1.25 and 2.5 μg/mL.

Conclusions: CRYAB exposure can be detected at the surface of human brain endothelial cells in response to irradiation. Pro-thrombotic CRYAB-targeting conjugates can bind under high flow conditions and in the presence of whole blood induce stable thrombus formation with high specificity and efficacy on irradiated surfaces. CRYAB provides a novel radiation marker for potential vascular targeting in irradiated brain AVMs.

1. Introduction

Vascular targeting (VT) is the selective delivery of bioactive molecules to a particular vascular environment to induce occlusion or ablation. The concept was initially developed to treat solid tumors with the goal to cause rapid shutdown of pathological tumor vessels through delivery of thrombotic agents to induce localized thrombosis and occlusion [1,2]. The inherent molecular differences between tumor endothelium and the normal endothelium make vascular targeting a good approach in cancer therapy, and targeted delivery to an array of discriminatory targets with various “coaguligands”, incorporating ligands such as antibodies or peptides attached to various effector molecules such as truncated tissue factor or thrombin, has been investigated [3–10].

Primary vascular pathologies, such as brain arteriovenous malformations (AVMs), could be amenable to this occlusive approach as these tangled collections of abnormal, rupture-prone vessels do not supply the brain, but instead act as arterio-venous shunts [11,12]. The

Abbreviations: AVM, arteriovenous malformations; CRYAB, αB-crystallin; FDP, fibrinogen degradation product; FITC, fluorescein isothiocyanate; Gy, Gray (unit); IgG, immunoglobulin; PS, phosphatidylserine; SRS, stereotactic radiosurgery; VT, vascular targeting

* Corresponding author at: Department of Clinical Medicine, Faculty of Medicine and Health Sciences, Level 1, 75 Talavera Rd, Macquarie University, Sydney, NSW 2109, Australia.
E-mail address: lucinda.mcrobb@mq.edu.au (L.S. McRobb).

https://doi.org/10.1016/j.thromres.2020.03.010
Received 20 January 2020; Received in revised form 23 February 2020; Accepted 13 March 2020
Available online 17 March 2020
0049-3848/

goal of AVM treatment is complete removal or occlusion of these pathological vessels to eliminate the risk of stroke. To date, inherent discriminatory endothelial targets have not been identified for VT of the AVM vasculature, hence stereotactic radiosurgery (SRS) has been suggested as a priming tool to induce a unique molecular signature on the AVM endothelium [13–18]. SRS has been used for more than three decades to manage patients with AVMs who are considered inappropriate for surgical resection [19]. Standard AVM radiosurgery achieves obliteration through a process of proliferation that leads to vessel wall remodeling and eventual closure [20], however the process suffers from long latency periods, is limited to small AVMs (< 25 mm diameter), and requires relatively high radiation doses [21]. The focused nature of SRS could allow molecular priming within the confines of the AVM nidus and in combination with VT provide a mechanism for focused and rapid induction of vessel occlusion, potentially with lower radiation doses, allowing therapy of large AVMs that are currently considered untreatable and reducing latency periods or incomplete occlusion from standard radiosurgery that leave patients at continued risk of stroke.

Radiation-induced targets including intercellular cell adhesion molecule-1 (ICAM-1), vascular cell adhesion molecule-1 (VCAM-1) and phosphatidylserine (PS), have been investigated pre-clinically in this context [17,22]. As endothelial targets, radiation-stimulated ICAM-1 and VCAM-1 suffer from lack of specificity in an AVM animal model [22], however greater success has been achieved with targeting of PS [17,][28]. Other putative surface targets have also been identified in recent proteomic studies [18,24,25]. One of these is the small heat shock protein, αB-crystallin (CRYAB). CRYAB normally acts as an intracellular chaperone to misfolded proteins in response to various cellular stresses, including radiation [26]. Importantly, studies in a rat AVM model and in cultured mouse brain endothelial cells demonstrated not only significant CRYAB induction in response to radiation but also evidence for translocation to the cell surface [25]. The absence of CRYAB on the normal endothelial surface in healthy cells and its unusual translocation to the endothelial surface after radiation suggests that this protein could potentially provide a highly discriminating target on radiation-primed cells.

In this study, we confirm the radiation-induced expression of CRYAB in the context of human brain endothelial cells and investigate surface-accessible CRYAB as a molecular target by creating an antibody-thrombin conjugate and assessing the efficacy and specificity of binding and thrombus formation in an established parallel-plate flow system with circulating whole blood.

2. Methods

2.1. Cell culture

The immortalized human cerebral microvascular endothelial cell line, hCMEC/D3 (CELLutions Biosystems Inc., Toronto, Canada), was cultured in EBM-2 medium (Lonza, Basel, Switzerland) supplemented with 5% fetal bovine serum, 1% penicillin/streptomycin, 10 mM HEPES (Life Technologies, Grand Island, NY), and 1 ng/mL human basic fibroblast growth factor (Sigma-Aldrich, North Ryde, Australia) at 37 °C in 5% carbon dioxide. Cells were passaged at 90% confluence with trypsin-EDTA (Life Technologies).

For flow studies, cells were seeded at 1×10^4 cells/mL onto collagen-coated 35 mm glass bottom petri dishes (MatTek Corporation, Ashland, MA) containing 1.5 mL complete EBM-2 medium and allowed to grow for 2 days to achieve 100% confluence. For immunostaining, cells were seeded at 1×10^4 cells/mL in collagen-coated 8-well chamber slides (Nunc Lab-Tek II, Sigma-Aldrich) in a final volume per well of 500 μL and grown to confluence prior to radiation or sham treatment.

2.2. Cell irradiation

Cells at confluence were irradiated by 6 MV linear accelerator (Elekta Synergy, Crawley, UK) at Macquarie University Hospital (Sydney, Australia) at three different doses (5, 15 or 25 Gy) as previously described [27]. Sham controls (0 Gy) were treated identically but were not irradiated. For this study, all immunostaining or flow studies were performed on cells 24 h after irradiation or sham treatment was given.

2.3. Immunocytochemistry

At 24 h after irradiation or sham treatment, cells in 8-well chamber slides were fixed briefly with 2% phosphate-buffered para-formaldehyde for 5 min without permeabilization. Fixed cells were blocked prior to addition of primary antibodies overnight at 4 °C. Primary antibodies to αB-crystallin (ab13496, mouse monoclonal IgG, Abcam, Cambridge, UK) and a non-specific mouse IgG control isotype (ab91353, Abcam) were used with an anti-mouse Alexa Fluor 647-tagged secondary antibody (A-31571, Thermofisher Scientific). A primary antibody to cleaved poly-ADP-ribose polymerase 1 (cleaved PARP-1, rabbit polyclonal IgG, STJ90100, St. John's Laboratories Ltd., London, UK) was used on fixed and permeabilized cells as an apoptotic marker with an anti-rabbit AF647-tagged secondary antibody (A-31573, Thermofisher Scientific). Cells were also co-stained with 4′,6-diamino-2-phenylindole dihydrochloride (DAPI, 5 μg/mL) for nuclear staining.

2.4. Fluorescent labelling of anti-CRYAB antibody for immunostaining under flow

For preliminary assessment of antibody binding to irradiated cells under flow, the anti-CRYAB antibody was pre-conjugated with a fluorophore and run in the parallel-plate flow system in the presence of medium rather than blood. Antibody-dye probes were prepared by conjugating Xenolight CF750 (Caliper Life Sciences Inc., Hopkinton, MA) to the anti-CRYAB and non-specific IgG antibodies according to the manufacturer's instructions (Fig. S1a). Briefly, 200 μg of each antibody was labelled by mixing with 0.04 nmol of dye in dimethylsulfoxide for 1 h at room temperature in the dark. Degree of labelling was calculated as 4 for both CRYAB and IgG antibody-dye probes under these conditions. The CF750-conjugated mouse IgG and anti-CRYAB at 1 μg/mL were used in the flow system in the presence of EBM-2 medium and circulated for a period of 15 min. The cells after flow were fixed and the nuclei stained before mounting for microscopic observation to assess binding using a Zeiss microscope with AxioCam HRc camera and Zen 2012 software (Carl Zeiss Microscopy, Jena, Germany).

2.5. Blood collection

All experimental procedures using human blood were approved by the Macquarie University Human Ethics Committee (approval number HREC: 5201300883) and were carried out according to the Australian Code of Practice for the Care and use of Human Tissues for Scientific Purposes (Version 4) with consent, as previously described [27]. A volume of 20 mL of human whole blood was collected at each sitting from healthy volunteers free from medication known to affect platelet function. The blood was drawn using standard venepuncture protocols into 4.5 mL tubes containing 3.2% buffered sodium citrate solution (BD Bioscience, San Jose, CA). Citrated blood was re-calcified just prior to use in the flow system using 10 mM $CaCl_2$ and 5 mM $MgCl_2$ in all experiments.

2.6. Conjugate preparation

Recombinant human thrombin (3.4 mg/mL, specific activity 3026

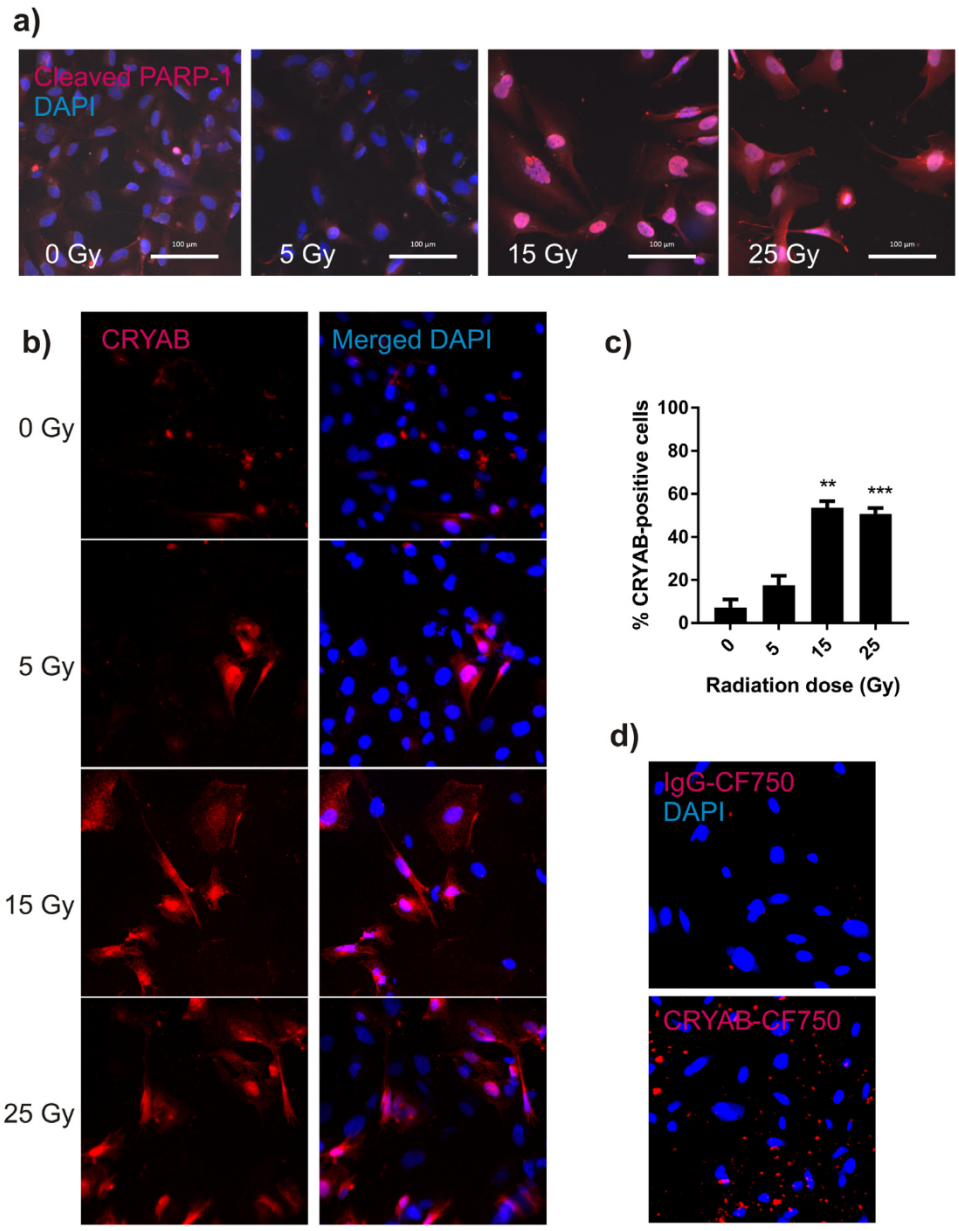

Fig. 1. CRYAB expression on hCMEC/D3 cells in response to radiation. (a) Representative images of permeabilized hCMEC/D3 cells stained with anti-cleaved PARP1 (AF647, red). Cells were stained 24 h after radiation at 0–25 Gy. Cells were co-stained with DAPI (blue) for nuclear localization. Bar 100 μm, magnification = 200×. (b) Representative immunostained images of fixed, non-permeabilized hCMEC/D3 cells taken 24 h after radiation (25 Gy) or sham (0 Gy) showing CRYAB expression (AF647, red). Cell nuclei were stained with DAPI (blue). (c) The percentage of CRYAB-positive cells per field of view was determined for three independent experiments. Data shown mean ± SD, one-way ANOVA with Dunnett's post-hoc, $^{**}p < 0.01$, $^{***}p < 0.001$, relative to sham-treated. (d) Representative images of CF750-IgG and CF750-anti-CRYAB binding to irradiated (25 Gy) endothelial cells under flow in the parallel-plate flow system using circulating EBM-2 medium. Cells were transferred to the flow system 24 h after irradiation or sham treatment. Conjugates were circulated for 15 min in the flow system prior to disassembly, fixation and imaging. CF750-tagged antibodies (red), cell nuclei stained with DAPI (blue). Magnification of all images, 200×. (For interpretation of the references to colour in this figure legend, the reader is referred to the web version of this article.)

NIH units/mg; Prospec, Israel) was conjugated with the anti-CRYAB antibody (ab13496, Abcam) using a Lys-Lys protein-protein conjugation kit (Click Chemistry Tools, Scottsdale, AZ, USA) according to the manufacturer's instructions. Briefly, 130 μL of thrombin (3.4 mg/mL) was labelled with 20-fold molar excess tetrazine (Tz) reagent and 100 μL anti-CRYAB or isotype IgG (1 mg/mL) in BUPH buffer (pH 7.5) was labelled with 20-fold molar excess trans-cyclooctene (TCO) reagent prior to conjugation (ratio 1:3). The conjugation reaction was monitored by SDS-PAGE (Fig. S1b) and residual thrombin activity of conjugate (80%, 2420 NIH units/mg) determined using a commercially available thrombin activity assay (AnaSpec, Fremont, CA).

2.7. Parallel–plate flow chamber

Set-up and operation of the parallel-plate flow chamber was as previously described [27] using a Glycotech flow chamber (Glycotech Co., Gaithersburg, ML) and pulsatile pump in an enclosed circulation system. The system was operated using flow parameters giving an average shear stress of 3.1 dynes/cm^2 (38 strokes/min; flow volume 2.4 mL/min; flow time 15 min), as previously established [27]. The flow chamber was assembled over a collagen-coated glass petri dish containing cultured cells 24 h after sham (0 Gy) or radiation (5, 15 or 25 Gy) treatment. A volume of approximately 12 mL of blood containing rhodamine 6G-labelled platelets (3 μg/mL) and FITC-labelled fibrinogen (130 μg/mL) was circulated through the system so that their deposition on the cell surface could be used as a measure of thrombus formation. Anti-CRYAB-thrombin was added to a final concentration of 1.25 or 2.5 μg/mL and the system operated for a period of 15 min. At the end of 15 min, the gasket was disassembled and the cells gently washed before Hoechst staining and fixation for microscopy. The post-flow blood was collected and plasma separated for analysis. Equivalent volumes of saline or concentration of IgG-thrombin were used as non-targeting controls.

2.8. Analysis of fibrinogen degradation product (FDP) in plasma

Plasma separated from whole blood was collected after flow by centrifugation at 1000 ×g for 10 min before enzyme-linked immunosorbent assay (ELISA) for fibrin degradation products (FDP) (Jomar Life Research, Scoresby, Victoria, Australia) as a further

measure of post-thrombotic events, as previously described [27].

2.9. Data and statistical analysis

Flow system imaging was performed with a Zeiss LSM880 Confocal Microscope and analyzed for platelet adhesion area and fibrin volume using 3D image reconstruction of Z stacks using Bitplane (IMARIS software, version 8), as described in detail previously [27]. Cells were viewed under bright-field and using ex358nm/em461nm for Hoechst, ex550nm/em570nm for rhodamine 6G-labelled platelets, and ex495/em519nm for fibrinogen-FITC. Five fields of view (200 × magnification) from each experiment were randomly selected and the average measurements were considered for analysis. Data analysis was performed using Prism 6.01 (Graphpad software Inc., La Jolla, CA). Values are given as mean ± standard deviation (SD) of three independent experiments. Multiple comparisons were performed using two-way ANOVA with Tukey's post-hoc analysis, or one-way ANOVA with Dunnet's post-hoc analysis for immunostaining analysis. P values < 0.05 were considered to be significant.

3. Results

3.1. Radiation induces CRYAB expression on human brain endothelial cells

Radiation induced some cell loss with some cellular hypertrophy and nuclear enlargement at the higher radiation doses as observed previously in this cell line [27] and in a bEnd3 mouse endothelial cell line [24] (Fig. 1). The caspase-target, cleaved PARP-1, was used as a marker of apoptosis and nuclear accumulation in fixed and permeabilized cells was observed at both 15 and 25 Gy on cells stained 24 h after irradiation (Fig. 1a). A similar dose-dependent pattern of CRYAB accumulation at the surface was also observed in fixed but non-permeabilized cells at the two higher doses (Fig. 1b, c).

3.2. CRYAB exposure allows targeted binding of antibodies under high flow

To further confirm CRYAB exposure at the surface and assess antibody binding in the presence of shear stress, fluorescently-tagged antibodies were introduced into the parallel-plate flow system in the presence of EBM-2 medium rather than blood. The binding efficiency of both targeted anti-CRYAB-CF750 and non-targeted IgG-CF750 on live irradiated endothelial cells under flow was analyzed by fluorescence microscopy at the highest radiation dose of 25 Gy. The CF750 fluorescent signal was evident on the endothelial cells exposed to radiation at 25 Gy using the anti-CRYAB-CF750 construct but minimal binding was observed with the IgG control (Fig. 1d). It was observed that the CRYAB-CF750 binding under flow was more punctate than observed after visualization by a standard immunostaining procedure. It is unclear why this difference may arise but may be due to differences in antibody concentration, incubation time, or the binding patterns that could be achieved under continuous flow within the 15 min in the parallel-plate system.

3.3. Anti-CRYAB-thrombin conjugate induces thrombus formation on irradiated cells

As CRYAB appeared a valid surface target, a conjugate was produced between the anti-CRYAB antibody and thrombin for testing in the parallel-plate flow system. Evidence for thrombus formation was observed by measuring platelet aggregation (aggregate size and number per field of view) (Fig. 2a, b) and fibrin deposition (aggregate size and number of deposits) (Fig. 2a, c), as described previously [27]. A dose-dependent response was observed for platelet accumulation in response to radiation for both conjugate concentrations (*i.e.* 1.25 μg/mL and 2.5 μg/mL) (Fig. 2b). In the absence of conjugate, no significant increases in platelet accumulation were observed. Statistical significance was reached at the highest radiation dose of 25 Gy for average platelet area compared to the irradiated and non-irradiated saline controls, but not for total platelet area.

As per our previous study, the lack of discriminatory power obtained with platelet measurement led us to examine fibrin deposition as a more reliable marker of stable thrombus formation (Fig. 2a, c) [27]. In saline controls, no fibrin deposition was observed on either irradiated or non-irradiated cells (Fig. 2c). No fibrin deposition was observed with either dose of conjugate in the absence of irradiation. In response to radiation there was a dose-dependent increase in fibrin deposition (both average and total fibrin volume) with both conjugate concentrations, reaching significance at 15 and 25 Gy with increases up to 24–53-fold greater than non-irradiated saline controls. No substantial fibrin deposition was observed at 5 Gy under any conditions.

We previously demonstrated that at the thrombin activity levels used in this study (0.36–0.6 NIH units/mL), untargeted, free thrombin does not induce significant fibrin accumulation in this system [27], hence these experiments were not repeated. Instead, an equivalent dose (0.6 NIH units/mL) of non-targeting IgG-thrombin was utilized as a more appropriate control to assess the targeting specificity of the CRYAB conjugate. These experiments were only performed at the highest radiation dose of 25 Gy where the most significant thrombus formation was observed (Fig. 3a–c) and were compared to the original CRYAB-thrombin dataset. In the presence of IgG-thrombin, minimal stimulation of platelet aggregation was observed in the absence of irradiation, as observed for the anti-CRYAB-thrombin conjugate (Fig. 3b). There was no significant increase observed in average and total platelet area in response to radiation at either IgG-conjugate dose compared to the non-irradiated control. Both average and total fibrin volume increased in response to IgG-thrombin in irradiated compared to non-irradiated cells, however the levels achieved were significantly lower than those achieved in response to the anti-CRYAB-thrombin conjugate, particularly at 25 Gy (Fig. 3c).

3.4. Plasma FDP measurements correlate with fibrin deposition

To further assess the maturity of the thrombi formed, the release of complex cross-linked fibrin degradation products (FDPs) in the post-flow plasma was measured after each experimental run in the parallel-flow system (Fig. 4). Significant increases were observed with both conjugate doses at a radiation dose of 15 Gy (16–22-fold) and 25 Gy (28 – 38fold). No significant increase in FDP level was noted at 5 Gy with either conjugate dose. This was in line with the lack of fibrin deposition observed. Post-flow plasma analysis of FDP correlated well with the extent of fibrin deposition observed in response to anti-CRYAB-thrombin. Interestingly however, no increase in FDP levels was observed in the presence of IgG-thrombin despite the observation of a moderate increase in fibrin accumulation.

4. Discussion

Our previous publication was the first to establish and test the parallel-plate flow system using phosphatidylserine (PS) as a target and annexin V as the targeting ligand [27]. The study demonstrated the utility of the system for ethically and economically verifying both targets and targeted coaguligands prior to animal studies and these findings have since been translated successfully to a preclinical AVM animal model [28]. However, as for many potential targets, levels of target expression or potential for off-target binding can necessitate a trade-off between targeting efficacy and specificity. Thus we continue to examine novel vascular targets induced by radiation priming that could be used either independently or in combination with PS in a dual targeting capacity. Hence, in this study, we used the established parallel-plate flow system to systematically approach the investigation of CRYAB as a novel vascular target. Using this system, we have now shown that: 1) CRYAB is up-regulated and accessible for binding at the endothelial

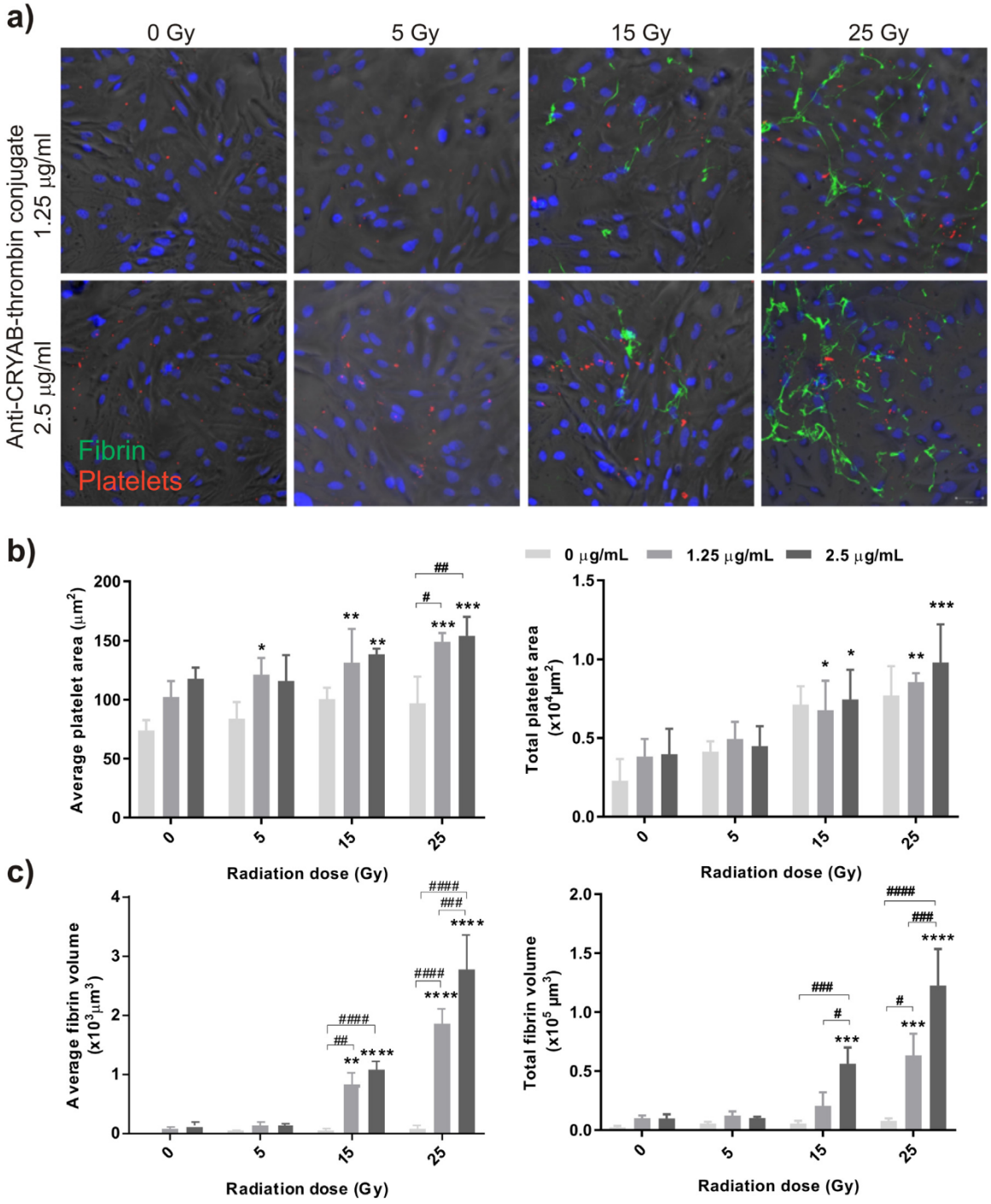

Fig. 2. Platelet aggregation and fibrin formation on irradiated endothelial cells in the presence of anti-CRYAB-thrombin conjugate. (a) Representative confocal images of platelet aggregation and fibrin formation on sham-irradiated (0 Gy) or irradiated endothelial cells (5, 15, or 25 Gy) in the parallel-plate flow system with 1.25 or 2.5 µg/mL conjugate. Thrombosis was assessed on cells 24 h post-irradiation or sham treatment. Conjugates were circulated in the system for 15 min to induce thrombosis. Platelets were pre-stained in whole blood with rhodamine 6G (red) and FITC-labelled fibrinogen (green) added prior to circulation. Cell nuclei were stained post-flow with Hoechst 33342 (blue); fluorescence is overlaid on brightfield images. Magnification = 200×. (b) Quantitative analysis of average size of platelet aggregates and total platelet area per field of view (μm^2); (c) Quantitative analysis of average fibrin volume and total fibrin volume per field of view (μm^3). Data are shown as mean ± SD (n = 3) and were analyzed using two-way ANOVA with Tukey's post-hoc analysis. ****p < 0.0001, ***p < 0.001, **p < 0.01, *p < 0.5 comparisons relative to saline, non-irradiated control. ####p < 0.0001, ###p < 0.001, ##p < 0.01, #p < 0.05 comparisons within radiation dose groups. (For interpretation of the references to colour in this figure legend, the reader is referred to the web version of this article.)

surface in response to radiation, and that this occurs reproducibly in human cells as well as animal cells; this has not previously been demonstrated; 2) thrombin can be delivered with high specificity to irradiated cells using a CRYAB-targeting antibody; CRYAB surface expression and antibody binding is of sufficient affinity to be maintained under flow and induce thrombosis in the presence of whole blood, however an expected degree of non-specific binding on irradiated cells should be considered in the development of antibody-based targeting conjugates going forward; 3) the absence of CRYAB and lack of binding and thrombus formation on non-irradiated human endothelial cells

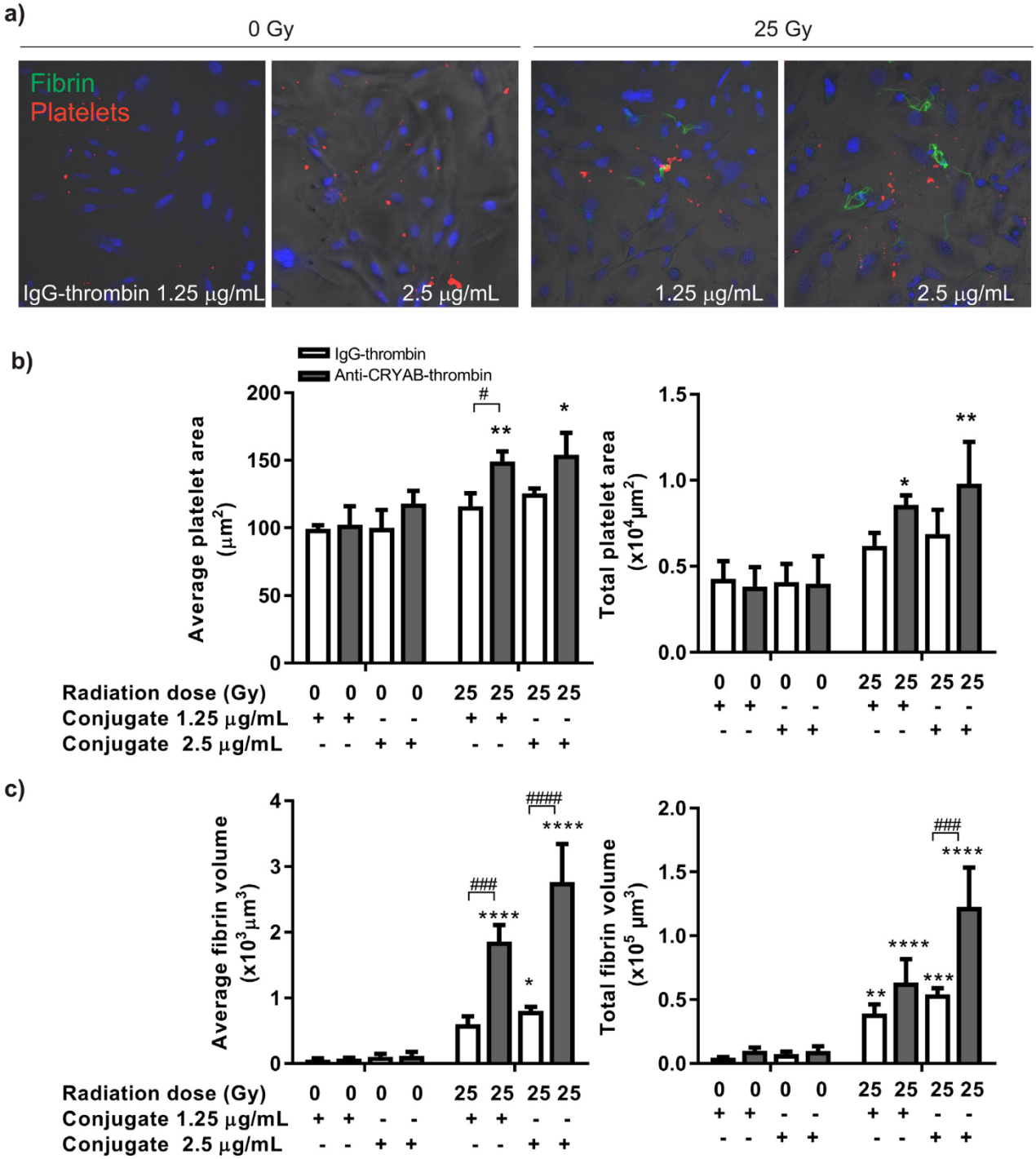

Fig. 3. Platelet and fibrin deposition in response to non-targeted IgG-thrombin conjugate. (a) Representative confocal images of platelet aggregation (μm^2, red) and fibrin formation (μm^3, green) on irradiated endothelial cells (25 Gy) or sham control (0 Gy) in the presence of IgG-thrombin conjugate compared to anti-CRYAB-thrombin at 1.25 or 2.5 μg/mL under flow. Thrombosis in the flow system was assessed on cells taken 24 h post-irradiation or sham treatment. Conjugates were circulated for 15 min in the flow system. Nuclei were stained with DAPI or Hoechst 33342 (blue; fluorescence is overlaid on brightfield images). Magnification, 200×. (b) Quantitative analysis of average platelet area and total platelet area per field of view (μm^2). (c) Quantitative analysis of average fibrin volume and total fibrin volume per field of view at 25 Gy for both conjugate doses (μm^3). Data are shown as mean ± SD ($n = 3$) and were analyzed using two-way ANOVA with Tukey's post-hoc analysis. $^{****}p < 0.0001$, $^{***}p < 0.001$, $^{**}p < 0.01$, comparisons relative to sham control. $\#p < 0.5$, comparisons relative to low conjugate dose within radiation dose group. (For interpretation of the references to colour in this figure legend, the reader is referred to the web version of this article.)

demonstrates the priming effect of radiation and the specificity of CRYAB as a potential radiation target in the vasculature. Collectively, these findings indicate that CRYAB could provide a highly discriminatory marker on radiation-primed endothelium and supports progression to *in vivo* studies.

CRYAB was initially identified as a putative target in a series of proteomic studies that examined surface exposure through biotin-labelling [18,24,25]. In a rat AVM model and a mouse endothelial cell line, both the absence of CRYAB on normal, non-irradiated endothelial cells and the up-regulation of CRYAB and surface exposure in response to radiation was validated [25]. Most studies report intracellular CRYAB accumulation in the cytoplasm and translocation to the nucleus

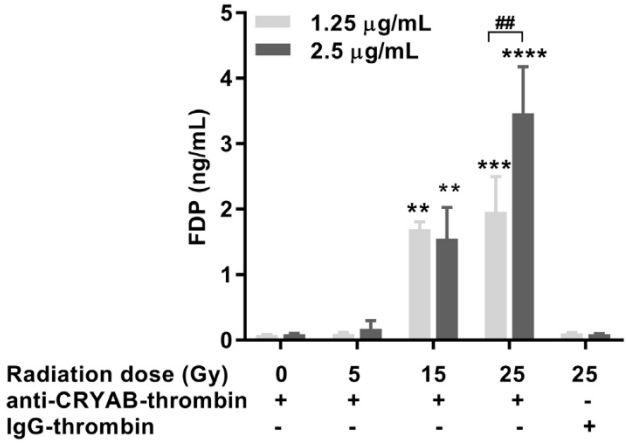

Fig. 4. Plasma fibrinogen degradation product (FDP) concentration after flow in the presence of conjugate. Presence of FDP (ng/mL) analyzed in plasma after treatment with 1.25 μg/mL and 2.5 μg/mL anti-CRYAB-thrombin conjugate (0–25 Gy) or 2.5 μg/mL IgG thrombin conjugate (at 25 Gy) in the parallel-plate flow system. After each 15 min run, plasma was separated from the whole blood containing conjugate from the circulation and analyzed for FDP presence by ELISA. Data are shown as mean ± SD (3 independent experiments). Statistical differences were analyzed using two-way ANOVA with Tukey's post-hoc analysis. ****$p < 0.0001$, ***$p < 0.001$, **$p < 0.01$ comparisons relative to non-irradiated control. ##p < 0.01, comparison relative to low conjugate dose within radiation dose.

or mitochondria in response to stress or under pathological conditions where it acts as a chaperone to bind misfolded or unfolded proteins to protect them from aggregation that may otherwise lead to cell toxicity and death [29–31]. CRYAB is also a normal resident of the eye lens where its chaperone-like activity prevents protein aggregation and lens cell death [32]. Less commonly, exosomal release of CRYAB has been observed in glioblastoma and from ischemic cardiomyocytes [33,34]. The mechanism by which CRYAB translocates to the surface of the vasculature in response to radiation remains unclear, however the absence of CRYAB on the normal endothelium and atypical surface localization in response to radiation support ongoing studies to further assess *in vivo* biodistribution in the vasculature and targeting in the context of AVM treatment.

Ideally, we would examine the molecular effects of radiation on CRYAB expression in human AVMs directly. However, we cannot ethically take AVM tissues from patients after they have undergone radiosurgery and gaining sufficient endothelial cells at early passage from surgically-excised human AVMs for radiation studies is challenging. Although significant subculture may irrevocably alter some phenotypic characteristics it is worth pursuing this in the future. Based on this study and our cumulative findings that radiation stimulates CRYAB in three species (rat, mouse, human) and in both brain endothelium as well as ex-cranial vasculature (rat model) [25], the phenomenon appears robust and repeatable, and theoretically transferrable to human AVM endothelium. Potential deviation from this effect in AVMs could derive from the activating-RAS genotype predominant in most AVMs [35] or potentially from flow-mediated effects on endothelial gene expression. However, RAS activation in cancer cells does not result in upregulation of basal CRYAB expression [36] and we have evidence from the rat AVM model that hemodynamic derangements do not induce CRYAB expression in the absence of radiation [25]. These findings are consistent with the predominant role of CRYAB as a damage-associated chaperone and give increased confidence in translation of CRYAB as a discriminatory target in an AVM setting. Overexpression of activated RAS in vascular endothelial cells could be used to examine this *in vitro*, and further biodistribution studies in pre-clinical models are required to assess any potential for off-target binding in other vascular beds, however collectively, our data suggests strong potential for radiation specificity at this stage.

We previously used the *in vitro* parallel-plate flow chamber to successfully examine PS as a radiation target with an annexin V-thrombin conjugate as the targeting coaguligand [27]. As observed for the CRYAB conjugate, the annexin V-thrombin conjugate demonstrated dose-dependent and synergistic thrombus induction in response to increasing radiation doses, with the higher combined dose of radiation (25 Gy) and conjugate (2.5 μg/mL) causing significantly greater thrombus formation compared to the lower doses with both conjugates. Similarly, significant induction was also observed with radiation doses of 15 Gy for both conjugates. In contrast, the annexin V-thrombin conjugate demonstrated low-level fibrin formation at 5 Gy, which was not apparent with the CRYAB conjugate. Binding differences and efficacy could be related to several variables such as: 1) the conjugate concentration, which was not truly equivalent given the size differential between annexin V (30 kDa) and the CRYAB antibody (150 kDa); 2) differences in ligand/antibody binding affinities for their targets; or 3) to differences in endothelial target expression at each dose. The latter is consistent with the lack of surface expression observed by immunostaining at this radiation dose. Ideally, identifying a target induced at a low radiation dose would improve the safety profile and potentially allow treatment of patients with large AVMs. Patients with AVMs up to 3 cm can be safely and effectively treated (up to 80% cure rate) with mean radiation doses typically within the 15–25 Gy range however this drops significantly for larger AVMs (< 18% cure rate) [37]. Combining this radiosurgery with VT could potentially improve cure rates in large AVMs and the induction of immediate thrombotic AVM occlusion could also remove the often long latency periods experienced by patients after standard radiosurgery that leave them vulnerable to stroke [38]. Our data still suggest the possibility of achieving selective vessel thrombosis by using anti-CRYAB conjugate at 15 and 25 Gy. While we cannot assume that this level of thrombosis observed in the *in vitro* system will translate *in vivo* without further pre-clinical studies, previous translation of equivocal flow system data for PS [27] to successful AVM vessel occlusion in an animal model [28] strengthens the argument for advancement of CRYAB conjugates to *in vivo* studies to assess whether CRYAB or PS, and their respective conjugates, make the better targets or targeting agents, with respect to selectivity and efficacy. Dual targeting to more than one biomarker with a combination of targeted coaguligands may also be a means of increasing efficacy while maintaining specificity [39].

Parallel-plate flow chambers are used to examine thrombosis *in vitro* as they simulate *in vivo* hemodynamic conditions and the forces that act upon early thrombus formation and stability [40,41]. While the shear stress of 3.1 dynes/cm^2 achieved in our system lies at the lower range of that found in AVM feeding vessels (2–67.4 dynes/cm^2) [42] because of the need to maintain cell attachment to the culture dish, the ability to circulate whole blood over the cell layer is not something that can be achieved in static cell conditions. It is a limitation however that we cannot assess higher shear rates at this stage and thus the necessity to move this molecule to an *in vivo* model. Parallel-flow chambers do provide however an economical and ethical way to test and compare combinations of radiation doses and conjugate concentrations prior to pre-clinical studies. We find that fibrin deposition provides a sensitive and reproducible measurement for thrombosis. Fibrinolysis and FDP formation often occur linearly with fibrin deposition. Increasing fibrin deposition itself stimulates plasminogen cleavage to plasmin, but it is the balance between thrombosis and fibrinolysis that determines the extent of clot formation [43]. Plasma FDP analysis is often used in humans as a marker and measure of disseminated intravascular coagulation (DIC). Our post-flow plasma analysis of FDP matched well with the extent of fibrin deposition observed, at least in the presence of the anti-CRYAB-thrombin conjugate. However, it was interesting that despite moderate fibrin deposition occurring in the presence of IgG-thrombin, no associated increase in FDP levels was observed. The low-level platelet activation and fibrin deposition may not have been

sufficient to produce the fibrin cross-linking characteristic of more complex thrombi or support subsequent reactivity of the fibrinolysis cascade. These findings further support the efficacy and specificity brought by the targeted conjugate to the irradiated cell surface. This is our second study using the parallel-flow system that found analysis of platelet binding was a poor marker of thrombus formation. While there were increasing trends in platelet binding consistent with the fibrin deposition, the analysis of triplicate experiments was not sufficient to see statistical significance consistently across all groups. The almost exponential increase in fibrin deposition appeared a far more robust and reliable marker of efficacy.

Overall, the findings reported a significant synergistic interaction between the effects of radiation and conjugate dose where the higher doses (25 Gy and 2.5 μg/mL) induced more effective thrombosis. While binding was observed in response to the IgG-thrombin non-targeting control, potentially due to construct interaction with endothelial Fc or thrombin receptors [44], the response was significantly greater in the presence of the anti-CRYAB conjugate, demonstrating CRYAB-specific binding was occurring. The lack of significant binding or thrombus formation on non-irradiated cells suggests the interaction was radiation-dependent and that specificity in the irradiated zone could be achieved despite the non-specific contribution. Potentially, development of humanized antibodies that lack the Fc region may provide greater targeting specificity as well as lower immunogenicity for antibody-conjugates, and the established *in vitro* flow system would be an ideal place to pre-test and compare such newly developed antibodies and test this hypothesis.

4.1. Summary and conclusion

The primary aim of this work was to validate CRYAB as an endothelial target on human cells after radiation; and subsequently develop and test the efficacy of a novel pro-thrombotic conjugate to CRYAB for assessing luminal accessibility and inducing thrombosis on irradiated endothelial cells under flow. The study demonstrated the successful validation and testing of a new molecular target, CRYAB, and its pro-thrombotic conjugate using a parallel-plate flow chamber under optimized shear-flow conditions. This work supports progression to preclinical animal studies for *in vivo* assessment of vascular CRYAB biodistribution and efficacy of the CRYAB-targeting conjugate in an AVM animal model and potentially for vascular targeting of irradiated tumors.

Supplementary data to this article can be found online at https://doi.org/10.1016/j.thromres.2020.03.010.

Funding sources

This work was supported by grants from the National Health and Medical Research Council of Australia (grant numbers: APP1047302; APP1085045).

Author contributions

Conception and design: SS, ZZ, GEG, VC, DWI, VM, MAS, LSM; Acquisition of data: SS, FF, LSM; Analysis and interpretation of data: SS, LSM; Drafting of article: SS, LSM; Critical revision of article: all authors; Funding acquisition: ZZ, GEG, MAS; Supervision: MAS, ZZ, LSM; Final approval: all authors.

Declaration of competing interest

The authors declare they have no conflict of interest.

References

[1] X. Huang, G. Molema, S. King, L. Watkins, T.S. Edgington, P.E. Thorpe, Tumor infarction in mice by antibody-directed targeting of tissue factor to tumor vasculature, Science. 275 (5299) (1997) 547–550, https://doi.org/10.1126/science.275.5299.547.
[2] P.E. Thorpe, Vascular targeting agents as cancer therapeutics, Clin Cancer Res. 10 (2) (2004) 415–427, https://doi.org/10.1158/1078-0432.ccr-0642-03.
[3] J. Denekamp, Endothelial cell proliferation as a novel approach to targeting tumour therapy, Br J Cancer. 45 (1) (1982) 136–139, https://doi.org/10.1038/bjc.1982.16.
[4] S. Ran, B. Gao, S. Duffy, L. Watkins, N. Rote, P.E. Thorpe, Infarction of solid Hodgkin's tumors in mice by antibody-directed targeting of tissue factor to tumor vasculature, Cancer Res. 58 (20) (1998) 4646–4653 doi: Published October 1998.
[5] F. Nilsson, H. Kosmehl, L. Zardi, D. Neri, Targeted delivery of tissue factor to the ED-B domain of fibronectin, a marker of angiogenesis, mediates the infarction of solid tumors in mice, Cancer Res. 61 (2) (2001) 711–716 doi: Published January 2001.
[6] S.S. Brack, L.M. Dinkelborg, D. Neri, Molecular targeting of angiogenesis for imaging and therapy, Eur J Nucl Med Mol Imaging. 31 (9) (2004) 1327–1341, https://doi.org/10.1007/s00259-004-1648-0.
[7] J. He, T.A. Luster, P.E. Thorpe, Radiation-enhanced vascular targeting of human lung cancers in mice with a monoclonal antibody that binds anionic phospholipids, Clin Cancer Res. 13 (17) (2007) 5211–5218, https://doi.org/10.1158/1078-0432.ccr-07-0793.
[8] R. Bieker, T. Kessler, C. Schwoppe, T. Padro, T. Persigehl, C. Bremer, J. Dreischaluck, A. Kolkmeyer, W. Heindel, R.M. Mesters, W.E. Berdel, Infarction of tumor vessels by NGR-peptide-directed targeting of tissue factor: experimental results and first-in-man experience, Blood. 113 (20) (2009) 5019–5027, https://doi.org/10.1182/blood-2008-04-150318.
[9] J. He, Y. Yin, T.A. Luster, L. Watkins, P.E. Thorpe, Antiphosphatidylserine antibody combined with irradiation damages tumor blood vessels and induces tumor immunity in a rat model of glioblastoma, Clin Cancer Res. 15 (22) (2009) 6871–6880, https://doi.org/10.1158/1078-0432.ccr-09-1499.
[10] Z.J. Huang, Y. Zhao, W.Y. Luo, J. You, S.W. Li, W.C. Yi, S.Y. Wang, J.H. Yan, Q. Luo, Targeting the vasculature of colorectal carcinoma with a fused protein of (RGD)(3)-tTF, ScientificWorldJournal. 2013 (2013) 637086, https://doi.org/10.1155/2013/637086.
[11] P. Moftakhar, J.S. Hauptman, D. Malkasian, N.A. Martin, Cerebral arteriovenous malformations. Part 1: cellular and molecular biology, Neurosurg Focus. 26 (5) (2009) E10, https://doi.org/10.3171/2009.2.focus09316.
[12] P. Moftakhar, J.S. Hauptman, D. Malkasian, N.A. Martin, Cerebral arteriovenous malformations. Part 2: physiology, Neurosurg Focus. 26 (5) (2009) E11, https://doi.org/10.3171/2009.2.focus09317.
[13] K. Storer, J. Tu, A. Karunanayaka, R. Smee, R. Short, P. Thorpe, M. Stoodley, Coadministration of low-dose lipopolysaccharide and soluble tissue factor induces thrombosis after radiosurgery in an animal arteriovenous malformation model, Neurosurgery. 61 (3) (2007) 604–611, https://doi.org/10.1227/01.neu.0000290909.32600.a8.
[14] S. Liu, V. Sammons, J. Fairhall, R. Reddy, J. Tu, T.T. Duong, M. Stoodley, Molecular responses of brain endothelial cells to radiation in a mouse model, J Clin Neurosci. 19 (8) (2012) 1154–1158, https://doi.org/10.1016/j.jocn.2011.12.004.
[15] R. Reddy, T.T. Duong, J.M. Fairhall, R.I. Smee, M.A. Stoodley, Durable thrombosis in a rat model of arteriovenous malformation treated with radiosurgery and vascular targeting, J Neurosurg. 120 (1) (2014) 113–119, https://doi.org/10.3171/2013.9.jns122056.
[16] Z. Zhao, M.S. Johnson, B. Chen, M. Grace, J. Ukath, V.S. Lee, L.S. McRobb, L.M. Sedger, M.A. Stoodley, Live-cell imaging to detect phosphatidylserine externalization in brain endothelial cells exposed to ionizing radiation: implications for the treatment of brain arteriovenous malformations, J Neurosurg. 124 (6) (2016) 1780–1787, https://doi.org/10.3171/2015.4.jns142129.
[17] N. Raoufi Rad, L.S. McRobb, Z. Zhao, V.S. Lee, N.J. Patel, A.S. Qureshi, M. Grace, J.J. McHattan, J.V. Amal Raj, H. Duong, S.R. Kashba, M.A. Stoodley, Phosphatidylserine Translocation after Radiosurgery in an Animal Model of Arteriovenous Malformation, Radiat Res. 187 (6) (2017) 701–707, https://doi.org/10.1667/rr14646.1.
[18] L.S. McRobb, V.S. Lee, M. Simonian, Z. Zhao, S.G. Thomas, M. Wiedmann, J.V. Raj, M. Grace, V. Moutrie, M.J. McKay, M.P. Molloy, M.A. Stoodley, Radiosurgery alters the endothelial surface proteome: externalized intracellular molecules as potential vascular targets in irradiated brain arteriovenous malformation, Radiat Res. 187 (1) (2017) 66–78, https://doi.org/10.1667/rr14518.1.
[19] D.Q. Sun, K.A. Carson, S.M. Raza, S. Batra, L.R. Kleinberg, M. Lim, J. Huang, D. Rigamonti, The radiosurgical treatment of arteriovenous malformations: obliteration, morbidities, and performance status, Int J Radiat Oncol Biol Phys. 80 (2) (2011) 354–361, https://doi.org/10.1016/j.ijrobp.2010.01.049.
[20] G.T. Szeifert, W.R. Timperley, D.M. Forster, A.A. Kemeny, Histopathological changes in cerebral arteriovenous malformations following Gamma Knife radiosurgery, Prog Neurol Surg. 20 (2007) 212–219, https://doi.org/10.1159/0000100119.
[21] W.A. Friedman, F.J. Bova, S. Bollampally, P. Bradshaw, Analysis of factors predictive of success or complications in arteriovenous malformation radiosurgery, Neurosurgery. 52 (2) (2003) 296–308, https://doi.org/10.1227/01.neu.0000043692.51385.91.
[22] N. Raoufi Rad, L.S. McRobb, V.S. Lee, D. Bervini, M. Grace, J. Ukath, J. McHattan, V.K.A. Sreenivasan, T.T.H. Duong, Z. Zhao, M.A. Stoodley, In vivo imaging of endothelial cell adhesion molecule expression after radiosurgery in an animal model

of arteriovenous malformation, PLoS One. 12 (9) (2017) e0185393, , https://doi.org/10.1371/journal.pone.0185393.
[24] L.S. McRobb, M.J. McKay, J.R. Gamble, M. Grace, V. Moutrie, E.D. Santos, V.S. Lee, Z. Zhao, M.P. Molloy, M.A. Stoodley, Ionizing radiation reduces ADAM10 expression in brain microvascular endothelial cells undergoing stress-induced senescence, Aging (Albany NY) 9 (4) (2017) 1248–1268, https://doi.org/10.18632/aging.101225.
[25] L.S. McRobb, M.J. McKay, A.J. Gauden, V.S. Lee, S. Subramanian, S.G. Thomas, M.K. Wiedmann, V. Moutrie, M. Grace, Z. Zhao, M.P. Molloy, M.A. Stoodley, Radiation-stimulated translocation of CD166 and CRYAB to the endothelial surface provides potential vascular targets on irradiated brain arteriovenous malformations, Int J Mol Sci. 20 (23) (2019), https://doi.org/10.3390/ijms20235830.
[26] N. Golenhofen, W. Ness, E.F. Wawrousek, D. Drenckhahn, Expression and induction of the stress protein alpha-B-crystallin in vascular endothelial cells, Histochem Cell Biol. 117 (3) (2002) 203–209, https://doi.org/10.1007/s00418-001-0378-7.
[27] S. Subramanian, S.O. Ugoya, Z. Zhao, L.S. McRobb, G.E. Grau, V. Combes, D.W. Inglis, A.J. Gauden, V.S. Lee, V. Moutrie, E.D. Santos, M.A. Stoodley, Stable thrombus formation on irradiated microvascular endothelial cells under pulsatile flow: pre-testing annexin V-thrombin conjugate for treatment of brain arteriovenous malformations, Thromb Res. 167 (2018) 104–112, https://doi.org/10.1016/j.thromres.2018.05.016.
[28] A.J. Gauden, L.S. McRobb, V.S. Lee, S. Subramanian, V. Moutrie, Z. Zhao, M.A. Stoodley, Occlusion of animal model arteriovenous malformations using vascular targeting, Transl Stroke Res. (2019), https://doi.org/10.1007/s12975-019-00759-y Epub [ahead of print].
[29] T. Iwaki, A. Iwaki, M. Miyazono, J.E. Goldman, Preferential expression of alpha B-crystallin in astrocytic elements of neuroectodermal tumors, Cancer. 68 (10) (1991) 2230–2240, https://doi.org/10.1002/1097-0142(19911115)68:10<2230::aid-cncr2820681023>3.0.co;2-7.
[30] T. Iwaki, A. Iwaki, J. Tateishi, Y. Sakaki, J.E. Goldman, Alpha B-crystallin and 27-kd heat shock protein are regulated by stress conditions in the central nervous system and accumulate in Rosenthal fibers, Am J Pathol. 143 (2) (1993) 487–495 doi: Published August 1993.
[31] R. Chis, P. Sharma, N. Bousette, T. Miyake, A. Wilson, P.H. Backx, A.O. Gramolini, alpha-Crystallin B prevents apoptosis after H2O2 exposure in mouse neonatal cardiomyocytes, Am J Physiol Heart Circ Physiol. 303 (8) (2012) H967–H978, https://doi.org/10.1152/ajpheart.00040.2012.
[32] K.L. Christopher, M.G. Pedler, B. Shieh, D.A. Ammar, J.M. Petrash, N.H. Mueller, Alpha-crystallin-mediated protection of lens cells against heat and oxidative stress-induced cell death, Biochim Biophys Acta. 1843 (2) (2014) 309–315, https://doi.org/10.1016/j.bbamcr.2013.11.010.
[33] J. Cubedo, G. Vilahur, L. Casani, G. Mendieta, E. Gomez-Jabalera, O. Juan-Babot, T. Padro, L. Badimon, Targeting the molecular mechanisms of ischemic damage: protective effects of alpha-crystallin-B, Int J Cardiol. 215 (2016) 406–416, https://doi.org/10.1016/j.ijcard.2016.04.072.
[34] R.A. Kore, E.C. Abraham, Inflammatory cytokines, interleukin-1 beta and tumor necrosis factor-alpha, upregulated in glioblastoma multiforme, raise the levels of CRYAB in exosomes secreted by U373 glioma cells, Biochem Biophys Res Commun. 453 (3) (2014) 326–331, https://doi.org/10.1016/j.bbrc.2014.09.068.
[35] S.I. Nikolaev, S. Vetiska, X. Bonilla, E. Boudreau, S. Jauhiainen, B. Rezai Jahromi, N. Khyzha, P.V. DiStefano, S. Suutarinen, T.R. Kiehl, V. Mendes Pereira, A.M. Herman, T. Krings, H. Andrade-Barazarte, T. Tung, T. Valiante, G. Zadeh, M. Tymianski, T. Rauramaa, S. Yla-Herttuala, J.D. Wythe, S.E. Antonarakis, J. Frosen, J.E. Fish, I. Radovanovic, Somatic Activating KRAS Mutations in Arteriovenous Malformations of the Brain, N Engl J Med. 378 (3) (2018) 250–261, https://doi.org/10.1056/NEJMoa1709449.
[36] M. Monticone, E. Biollo, M. Maffei, A. Donadini, F. Romeo, C.T. Storlazzi, W. Giaretti, P. Castagnola, Gene expression deregulation by KRAS G12D and G12V in a BRAF V600E context, Mol Cancer. 7 (2008) 92, https://doi.org/10.1186/1476-4598-7-92.
[37] B.A. Gross, R. Du, Surgical and radiosurgical results of the treatment of cerebral arteriovenous malformations, J Clin Neurosci. 19 (7) (2012) 1001–1004, https://doi.org/10.1016/j.jocn.2012.01.004.
[38] J.C. Flickinger, B.E. Pollock, D. Kondziolka, L.D. Lunsford, A dose-response analysis of arteriovenous malformation obliteration after radiosurgery, Int J Radiat Oncol Biol Phys. 36 (4) (1996) 873–879, https://doi.org/10.1016/s0360-3016(96)00316-1.
[39] F. Thoreau, L. Vanwonterghem, M. Henry, J.L. Coll, D. Boturyn, Design of RGD-ATWLPPR peptide conjugates for the dual targeting of alphaVbeta3 integrin and neuropilin-1, Org Biomol Chem. 16 (22) (2018) 4101–4107, https://doi.org/10.1039/c8ob00669e.
[40] C. Zhang, S. Neelamegham, Application of microfluidic devices in studies of thrombosis and hemostasis, Platelets. 28 (5) (2017) 434–440, https://doi.org/10.1080/09537104.2017.1319047.
[41] R. Van Kruchten, J.M. Cosemans, J.W. Heemskerk, Measurement of whole blood thrombus formation using parallel-plate flow chambers - a practical guide, Platelets. 23 (3) (2012) 229–242, https://doi.org/10.3109/09537104.2011.630848.
[42] A. Alaraj, S.F. Shakur, S. Amin-Hanjani, H. Mostafa, S. Khan, V.A. Aletich, F.T. Charbel, Changes in wall shear stress of cerebral arteriovenous malformation feeder arteries after embolization and surgery, Stroke. 46 (5) (2015) 1216–1220, https://doi.org/10.1161/strokeaha.115.008836.
[43] J.C. Chapin, K.A. Hajjar, Fibrinolysis and the control of blood coagulation, Blood Rev. 29 (1) (2015) 17–24, https://doi.org/10.1016/j.blre.2014.09.003.
[44] J. Wang, H. Zheng, X. Ou, C.M. Albertson, L.M. Fink, J.M. Herbert, M. Hauer-Jensen, Hirudin ameliorates intestinal radiation toxicity in the rat: support for thrombin inhibition as strategy to minimize side-effects after radiation therapy and as countermeasure against radiation exposure, J Thromb Haemost. 2 (11) (2004) 2027–2035, https://doi.org/10.1111/j.1538-7836.2004.00960.x.